

Reconstructing cosmic evolution with a density parametrization

Ritika Nagpal^{id,*}, Shibesh Kumar Jas Pacif^{id,†} and Abhishek Parida^{id,‡}

(Dated: March 29, 2022)

The current paper provides a comprehensive examination of a dark energy cosmological model in the classical regime, in which a generic scalar field is regarded as a dark energy source. Einstein's field equations are solved in model independent way i.e. using a scheme of cosmological parametrization. A parametrization of the density parameter as a function of the cosmic scale factor has been investigated in this line. The result is noteworthy because it shows a smooth transition from a decelerating to an accelerating phase in the recent past. The model parameters involved in the functional form of the parametrization approach utilized here were constrained using certain external datasets. The updated Hubble datasets containing 57 datapoints, 1048 points of recently compiled Pantheon datasets, and also the Baryon Acoustic Oscillation (BAO) datasets are used here to determine the best-fitting model parameter values. The expressions of several significant cosmological parameters are represented as a function of redshift 'z' and illustrated visually for the best fit values of the model parameters to better comprehend cosmic evolution. The obtained model is also compared with the Λ CDM model. Our model has a distinct behavior in future and shown a big crunch type collapse. The best fit values of the model parameters are also used to compute the current values of several physical and geometrical parameters, as well as phase transition redshift. To examine the nature of dark energy, certain cosmological tests and diagnostic analyses are done on the derived model.

I. INTRODUCTION

Before 1916, gravity was assumed to be an intrinsic property of objects - a constant instantaneous force that could act over long distances. But, the intriguing discovery of Einstein's theory of general relativity (GR) has changed the course of scientific history. GR solved the riddle of mercury's precision and explained that gravity was not a mysterious force acting at a distance in the background of space and time but resulted from bending the background itself. The key insight of the GR is that the shortest path between any two distant objects in the space is always curved. This curved geometry is the basis of GR. Scientist's paradigm about the cosmos has wholly changed after Einstein's theory of gravity over the past 100 years. Einstein's field equations (EFEs) have expressed many things analytically, and somehow this theory matched the observations, which had been a mystery for decades. Many skepticisms still present after 100 years of Einstein's GR, such as its inability to explain the singularities inside the black holes, big bang, age of the Universe and few more [1]. One of GR's biggest challenges is, understanding the curvature singularities, geodesic incompleteness, and b-incompleteness. Many inherent features of the Universe have led to plenty of consequences and conjecture in the field of GR. Therefore, one of the major pursuits in physics is finding a better theory. The Einstein's theory axed with theoretical as well as observational issues several times in the past century. However, new gravitational wave findings and a black hole image enhance GR's foundation. So, we are interested here to explore the late evolution of the Universe in the background of GR.

The present scenario with the expanding Universe is that it has gone through a series of evolution processes after the big bang where the two phases of accelerating expansion of the Universe play some major role. The first phase of cosmic acceleration is known as *inflation* (that occurred just after the big bang) and the second phase is the recently discovered *late-time acceleration* [2], [3], [4], [5]. The detection of Type Ia Supernovae (SNeIa) [2] provided the first evidence for cosmic acceleration in 1998. Afterward, many other observations have revealed strong support for the cosmic acceleration at late-times [6] and many others support this fact indirectly [7], [8] [9], [10], [11]. This cosmic speed-up bring about either the finding for a mysterious energy content of the space-time or for modifications in GR that could confront with such a concealed feature of the Universe. A negative pressure fluid must be introduced into the Universe's energy content to retain GR with acceleration in the classical regime. The term cosmological

* ritikanagpal.math@gmail.com

† shibesh.math@gmail.com

‡ abhishekparida22@gmail.com

constant Λ (a tiny number $\approx 1.3 * 10^{-52} m^{-2}$) into the Einstein field equations describes the intrinsic energy density of the vacuum, which plays the role of the most intriguing candidate of dark energy (DE). However, the mathematical expression Λ edges to a massive variation between the theoretical and observation predictions [12]. Many DE models [13] have been created as a result of the variety caused by the issue of fine-tuning and the cosmic coincidence problem related with CDM. A phenomenological solution of these issues with the standard model can be figured out by considering a cosmological term varying with time [14], [15]. Thus, the scalar field models have gained high popularity in recent decades as they play a crucial role in describing both early and late time cosmic acceleration by acting as a DE candidate [16]. The motivation of interest in this paper is to develop a cosmological model in terms of a scalar field that unifies the characteristic of scalar field cosmologies. A dynamically evolving scalar field can be utilized as a candidate of dark energy. A cosmological constant can be a slow roll scalar field. Other dark energy models with a general scalar field include quintessence [17], [18], [19], phantom [20], [21], [22], [23], K-essence [24], [25], [26], [27], quintom [28], [29], [30] etc., which can explain the Universe's evolution nicely. Few other candidates are tachyon scalar field [31], [32], [33] chameleon [34], [35], [36] scalar field, [37], [38], [39] etc. The theory is that the field must exert a lot of negative pressure in order to speed up the expansion of the Universe. The exotic fluid such as Chaplign gas [40], Polytrropic gas [41] can act as the candidates of dark energy. However, we are discussing a model in a model-independent way and are using a generic scalar field.

In the literature, the model-independent technique (or cosmological parametrization) of reconstructing a cosmological model with or without dark energy has been employed to fit data to the cosmic evolution of the Universe. The model independent approach in the framework of some DE candidates is of great interest nowadays and was first discussed by Starobinsky [42]. A broad variety of parametrization schemes [43] have been proposed in the literature to explain the development of the Universe, including the shift from early deceleration to late acceleration. Moreover, there are other parametrization schemes such as density parametrization, pressure parametrization together with the parametrization of deceleration parameter, Hubble parameter, Scale factor and more (For a detailed list of parametrization schemes see [43]). Therefore, the purpose of this paper is to advocate for a particular parametrization of the scalar field's energy density, which better explains cosmic dynamics and provides more compact limitations than any other cosmological parameter.

This paper's work has been arranged as follows: Section I gives a quick overview of general relativity and the present state of some of the most pressing cosmological issues. The basic set up of scalar field as a candidate for dark energy in GR is explored in Sect. II. In Sect. III, we consider the space-time metric and formulated the Einstein Field equations in GR. We got the solutions to field equations using a basic parametrization approach in Sect. IV. In Sect. V, we have constrained the model parameters involved in our model using some external datasets and found the best fit values of some cosmological parameters. In Sect. VI, some detailed analysis of the model through the behavior of physical parameters through graphical representation are discussed. We examined the feasibility of our model via energy conditions in Sect. VII, and we wrap up our findings in Sect. VIII.

II. BASIC FORMALISM WITH A GENERAL SCALAR FIELD

Since, dark energy has been a mystery until now and because of a lack of understanding of the matter sector, selecting a suitable candidate for dark energy is a difficult undertaking. However, it is generally represented by a x-matter or a large-scale scalar field ϕ . So, in this paper, we will examine an ordinary scalar field with the Lagrangian density $L = -\frac{1}{2}g^{\mu\nu}\partial_\mu\phi\partial_\nu\phi - V(\phi)$ that is minimally related to gravity (technically known as quintessence field), then the gravitational action for the scalar field will be given by,

$$S = \int d^4x \sqrt{-g} \left[-\frac{1}{2}g^{\mu\nu}\partial_\mu\phi\partial_\nu\phi - V(\phi) \right], \quad (1)$$

where $V(\phi)$ denotes the scalar field's potential. Because dark energy is supposed to be homogenous, we may consider the scalar field to be spatially homogeneous, in which case the scalar field's stress-energy tensor also assumes the form of a perfect fluid and can be expressed as,

$$T_{\mu\nu}^\phi = T_{\mu\nu}^{Dark\ Energy} = (\rho_\phi + p_\phi) U_\mu U_\nu + p_\phi g_{\mu\nu}. \quad (2)$$

Where ρ_ϕ and p_ϕ respectively represent the scalar field's energy density and pressure. The wave equation governs the temporal development of the scalar field and is given by,

$$\ddot{\phi} + 3H\dot{\phi} + \frac{dV(\phi)}{d\phi} = 0. \quad (3)$$

A derivative with regard to time t is represented by an overhead dot from now on. Einstein's gravitational field equations are as follows:

$$R_{\mu\nu} - \frac{1}{2}Rg_{\mu\nu} = -8\pi GT_{\mu\nu}, \quad (4)$$

with $c = 1$, where $T_{\mu\nu} = (\rho + p)U_\mu U_\nu + p g_{\mu\nu}$ represents the Universe's ideal source of fluid matter (perfect fluid). With the introduction of dark energy into the Einstein field equations, the energy momentum tensor $T_{\mu\nu}$ will be modified to $T_{\mu\nu}^{Total}$, where

$$T_{\mu\nu}^{Total} = T_{\mu\nu}^{Matter} + T_{\mu\nu}^{Dark\ Energy} = (\rho_{Total} + p_{Total}) U_\mu U_\nu + p_{Total} g_{\mu\nu} \quad (5)$$

By considering the low contribution of baryons and radiation, we write $\rho_{Total} = \rho_m + \rho_\phi$ and $p_{Total} = p_m + p_\phi$. Here, ρ_m and p_m are respectively, the energy density and pressure of the dark matter in the Universe. Since the dark matter pressure is negligible, we take $p_m \approx 0$. In the next section, we shall apply this set up to a specific metric space and find the solution of EFEs.

III. EINSTEIN FIELD EQUATIONS

To begin, let us suppose that the Universe is homogenous and isotropic. So, we will use the Friedmann-Lemaitre-Robertson-Walker space-time with flat geometry as the backdrop metric in the form,

$$ds^2 = dt^2 - a^2(t)(dx^2 + dy^2 + dz^2), \quad (6)$$

$a(t)$ denotes the Universe's scale factor. With the above matter source description in the Universe, the Friedmann equations can be represented in the form,

$$\rho_{Total} = 3M_{pl}^2 H^2, \quad (7)$$

$$\rho_{Total} + 3p_{Total} = 6M_{pl}^2 H^2 q, \quad (8)$$

where, $H \left(= \frac{\dot{a}}{a} \right)$ and $q \left(= -\frac{a\ddot{a}}{\dot{a}^2} \right)$ are Hubble parameter and deceleration parameter respectively and $M_{pl} = (8\pi G)^{-1/2}$ is the Planck mass. If we consider the effective equation of state as $p_{Total} = \omega_{Total}\rho_{Total}$ then it is easy to write,

$$q = \frac{1}{2} (1 + 3\omega_{Total}) \quad (9)$$

From equations Eq. (7) and Eq. (8), the total conservation equation can be derived as,

$$\dot{\rho}_{Total} + 3H(\rho_{Total} + p_{Total}) = 0 \quad (10)$$

Two scenario comes into picture now. Either matter field and scalar field interact gravitationally or have minimal interaction. Let us consider the interaction between the two fields is minimal which leads to

$$\dot{\rho}_m + 3H(\rho_m + p_m) = 0 \quad (11)$$

$$\dot{\rho}_\phi + 3H(\rho_\phi + p_\phi) = 0 \quad (12)$$

Since, the dark matter pressure is negligible, we have $p_m = 0$, the above equation Eq. (11) yield $\rho_m = c_1 a^{-3}$, where c_1 is a constant of integration.

The energy density and pressure for the scalar field under consideration in the FLRW backdrop may be expressed as,

$$\rho_\phi = \frac{\dot{\phi}^2}{2} + V(\phi), p_\phi = \frac{\dot{\phi}^2}{2} - V(\phi). \quad (13)$$

Here, $\frac{\dot{\phi}^2}{2}$ and $V(\phi)$ are respectively the kinetic term and potential term for the field respectively. If the potential term dominates over the kinetic term i.e. $\dot{\phi}^2 \ll V(\phi)$ (slow roll scalar field), then the equation of state parameter w_ϕ ,

$$w_\phi = \frac{\frac{\dot{\phi}^2}{2} - V(\phi)}{\frac{\dot{\phi}^2}{2} + V(\phi)} = \frac{-1 + \frac{\dot{\phi}^2}{2V}}{1 + \frac{\dot{\phi}^2}{2V}} \quad (14)$$

resumes the value to $w_\phi = -1$ and then the potential term would behave like a cosmological constant Λ . we must mention here that, most favoured candidate of dark energy is the Einstein's cosmological constant Λ and Λ CDM model has the nice fits to most of the observational datasets. However, for the dynamical case, the values of w_ϕ ranges between -1 and $+1$ and discuss some other candidates of DE (see [16]). In the next section, we shall discuss the solution in case of dynamical w_ϕ .

IV. SOLUTION OF FIELD EQUATIONS

From equation Eq. (12), we can write

$$\rho_\phi = c_2 \exp \left[-3 \int H(1 + \omega_\phi) dt \right], \quad (15)$$

where c_2 is a constant of integration. For if $\omega_\phi = \text{constant}$, a particular case of slow roll scalar field (cosmological constant), Eq. (15) yield $\rho_\phi = c_2 a^{-3(1+\omega_\phi)} = \text{constant}$. But, we are considering here the dynamic equation of state for the scalar field, i.e. $\omega_\phi \neq \text{constant}$ that serves as a candidate of dynamical dark energy (ϕ varies with time t) and describes the late time cosmic acceleration. In this scenario, the scalar field ϕ is the only source of dark energy having potential $V(\phi)$ that interacts with itself. Eq. (15) can also be represented as,

$$\omega_\phi = -1 - \frac{1}{3} a \frac{\rho_\phi'}{\rho_\phi}, \quad (16)$$

where the prime denotes the derivative *w.r.t.* the scale factor a . In order to solve above system of equations, which contains only three independent equations with four unknowns a , ρ_m , ρ_ϕ and p_ϕ , we need an additional constraint equation. As discussed in the introduction about the model independent way or the cosmological parametrization scheme, here we assume an appropriate parametrization of ρ_ϕ of the form,

$$\rho_\phi = (a)^\beta \left[\cosh^{-1} \left(\frac{1}{\beta * a} \right) \right]^\alpha \quad (17)$$

where $\alpha \in (0, 1)$ and $\beta \in (0, 1)$ are two model parameters which can be constrained from some observational datasets.

The selection of ρ_ϕ is made in such a way that the term $\cosh^{-1}\left(\frac{1+z}{\beta}\right)$ can generate a signature flip behavior of equation of state parameter. Thus, the equation in (17) indicates a concave downward movement (i.e. the gradient decreases at each point over time t). There are various mathematical forms of these types of parametrization in literature (see [43], where different parametrization schemes used in the past few decades are summarized in detail), which help to study different dark energy models, which are capable of explaining some features of the observational cosmology. The most interesting characteristic of this model independent way study is that, it does not presuppose or influence the validity of gravitational theory nor they violate the physical and geometric properties [12] rather it provides some satisfactory explanation to different scenarios coming from observation and reconstruct the evolution of the Universe. The important point in any parametrization scheme is that the new functional form assumed contain some free parameters (model parameters), which should be chosen properly and can be done by constraining the model with some observational datasets. For this, it is better to write the expressions of cosmological parameters in terms of redshift z . For a detailed study of these kinds of model building/ reconstructions, one can refer to some recent papers [44], [45], [46], [47], [48], [49], [50], [51] in different scenarios.

Using the relation of redshift z and scale factor a given by $\frac{a}{a_0} = \frac{1}{(1+z)}$, where a_0 is the present (t_0 or $z = 0$) value of scale factor and normalized to $a_0 = 1$. We have then $\rho_m = \rho_{m0}(1+z)^3$, (where $\rho_{m0} = \rho_m(z=0) = \rho_m(t_0)$ is the current value of the energy density of dark matter). Now, the energy density of scalar field ρ_ϕ in terms of redshift reads as,

$$\rho_\phi(z) = (1+z)^{-\beta} \left\{ \cosh^{-1} \left(\frac{1+z}{\beta} \right) \right\}^\alpha, \quad (18)$$

with $\rho_{\phi 0} = \rho_{\phi 0}(z=0) = \left[\cosh^{-1} \left(\frac{1}{\beta} \right) \right]^\alpha$ being the current value of the energy density of scalar field and we can write $\rho_\phi(z)$ as,

$$\rho_\phi(z) = \rho_{\phi 0} (1+z)^{-\beta} \frac{\left\{ \cosh^{-1} \left(\frac{1+z}{\beta} \right) \right\}^\alpha}{\left\{ \cosh^{-1} \left(\frac{1}{\beta} \right) \right\}^\alpha} \quad (19)$$

Further, the Friedmann equation Eq. (7) can be written as,

$$3M_{pl}^2 H^2(z) = \rho_{m0}(1+z)^3 + \rho_{\phi 0} \left\{ \cosh^{-1} \left(\frac{1}{\beta} \right) \right\}^{-\alpha} (1+z)^{-\beta} \left\{ \cosh^{-1} \left(\frac{1+z}{\beta} \right) \right\}^\alpha \quad (20)$$

Let us now introduce the density parameter $\Omega = \frac{\rho}{\rho_c}$, which describe the whole content of the Universe, where ρ_c is the critical density of the Universe and $\rho_c = \frac{3H^2}{8\pi G} = 3M_{pl}^2 H^2$.

Equation Eq. (20) in terms of density parameter of matter and scalar field can be expressed as,

$$H(z) = H_0 \left[\Omega_{m0}(1+z)^3 + \Omega_{\phi 0} \left\{ \cosh^{-1} \left(\frac{1}{\beta} \right) \right\}^{-\alpha} (1+z)^{-\beta} \left\{ \cosh^{-1} \left(\frac{1+z}{\beta} \right) \right\}^\alpha \right]^{\frac{1}{2}}, \quad (21)$$

where $\Omega_{m0} = \frac{\rho_{m0}}{3M_{pl}^2 H_0^2}$ and $\Omega_{\phi 0} = \frac{\rho_{\phi 0}}{3M_{pl}^2 H_0^2}$ are the present values of matter and scalar field density parameters respectively.

The obtained model is described by the Eq. (21) with the model parameters α & β and the density parameters Ω_{m0} & $\Omega_{\phi0}$ which can be constrained using some observational datasets. In the next section, we have constrained these model parameters using some available external datasets such as Hubble datasets, Pantheon datasets and Baryon Acoustic oscillation datasets and found the best fit values of them for further analysis and discussed the behavior of other physical and geometric parameters of the model.

V. STATISTICAL ANALYSIS OF THE MODEL PARAMETERS

The advancement in observational cosmology allow us to understand the ancient and late cosmic evolution, the properties of dark components in the Universe along with the structure formation. The past three decades of cosmic studies (following Hubble's space telescope) in observational cosmology have yielded an enormous amount of observational datasets, such as SDSS, which produces a map of galaxy distribution and encodes current variations in the Universe, CMBR, which verifies the big bang theory, QUASARS, which clarifies the matter between observer and quasars, and BAO, which estimates large scale structures in the Universe to better interpret the DE. And also the SNeIa observations (known as standard candles) which are the devices for computing the cosmic distances and many more. So, in this part, we use error bar plots of Hubble datasets and *SNeIa* Pantheon datasets to compare our model to the Λ CDM model, and we use statistical analysis to restrict the values of model parameter & included in our model using *Hubble*, *Pantheon*, and *BAO* datasets.

In this paper, we advocated for using Python's scipy optimization technique to restrict the value of model parameters and anticipate the global minima of Hubble function mentioned in Eq. (21). The impressive fluctuations within the inclining diagonal components of the covariance matrix relating to the parameters are noticed. By employing the aforesaid measurements as means and a Gaussian prior with a fixed value $\sigma = 1.0$ as the dispersion, we used Python's emcee module for the mathematical research and numerical analysis. Thus, we examined the parameter space encompassing the local minima. The results are displayed as two-dimensional contour plots with $1 - \sigma$ and $2 - \sigma$ errors. Also, the strategy utilized with these datasets are talked about in details below.

A. Hz datasets

The Hubble parameter H is one of the most crucial cosmic parameter that explains the expansion rate in the Universe. It contains the necessary information on the cosmic history. The Hubble parameter in terms of some physical quantities such as redshift, length and time can be expressed as, $H(z) = -\frac{1}{1+z} \frac{dz}{dt}$, where dz is the outcome of spectroscopic surveys and the term dt gives the model-independent value of $H(z)$. The observations from the parameter $H(z)$ highlight the dark ages of the Universe such as issues based on dark matter and dark energy .

There are two elemental arrangements which are greatly used in literature to estimate the value of $H(z)$ at any instant z :

- (1) The extraction of $H(z)$ from BAO data
- (2) The differential age methodology [52]-[70].

In this article, we have taken the updated list of datasets to 57 points (i.e. 31 and 26 one from the differential age approach and other from the BAO and some different strategies respectively) between the range of redshift $z \in [0.07, 2.42]$ [71]. Although there is discrepancy in choosing the value of Hubble parameter (known as Hubble tension), here we have taken $H_0 = 69 \text{ Km/s/Mpc}$ for our analysis.

The observational constraints on the model parameters α and β (proportionate to the highest probability examination) can be captured by minimizing the chi-square value (χ^2_{min}), i.e. is equivalent to say the maximum likelihood analysis. The likelihood function $\chi^2_H(\alpha, \beta, \Omega_{m0}, \Omega_{\phi0})$ can be computed as:

$$\chi^2_H(\alpha, \beta, \Omega_{m0}, \Omega_{\phi0}) = \sum_{i=1}^{57} \frac{[H_{th}(z_i, \alpha, \beta, \Omega_{m0}, \Omega_{\phi0}) - H_{obs}(z_i)]^2}{\sigma_{H(z_i)}^2},$$

where H_{obs} and H_{th} assume the role of the observed and theoretical value of H respectively. Also, $\sigma_{H(z_i)}$ indicate the standard error in the value of H so observed. Table-1 expresses 57 points of $H(z)$ with corresponding errors σ_H along with the references.

B. Pantheon datasets

As we move into the advancement of technology, we study observational cosmology through various datasets which discuss various certainties in observational cosmology (e.g., early evolution, structure formation, and secrets of the dark Universe that somehow explain the late-time cosmic acceleration employing cosmic mechanism and ray detectors). Among the various observational datasets, the pantheon sample is one of the most significant datasets, which contains 1048 data points, and is the foremost discharged supernovae type Ia datasets.

Pantheon datasets points [72] of spectroscopically wrap the range of redshift z in the interval $z \in (0.01, 2.26)$. The outcome of these datasets provide the assessment of the distance moduli $\mu_i = \mu_i^{obs}$ in the range of redshift $z \in (0, 1.41]$

The distance moduli can be obtained by the equation $\mu_i^{th} = \mu(D_L) = m - M = 5 \log_{10}(D_L) + \mu_0$. The associated terms M , m and μ_0 in this equation are represented as absolute magnitude, apparent magnitude and marginalized nuisance parameter respectively. Also, μ_0 can be calculated as $\mu_0 = 5 \log \left(H_0^{-1} / Mpc \right) + 25$. To identify the best match of the model parameters α , β and cosmological parameters Ω_{m0} & $\Omega_{\phi0}$ of the developed model, the theoretical value of the distance modulus (μ_i^{th}) can be compared with the observed value of distance modulus (μ_i^{obs}). By the above data, the formula of luminosity distance can be adjusted as:

$$D_l(z) = \frac{c(1+z)}{H_0} S_k \left(H_0 \int_0^z \frac{1}{H(z^*)} dz^* \right),$$

$$\text{where } S_k(x) = \begin{cases} \sinh(x\sqrt{|\Omega_k|}) / \Omega_k, & \Omega_k > 0 \\ x, & \Omega_k = 0 \\ \sin x\sqrt{|\Omega_k|} / |\Omega_k|, & \Omega_k < 0 \end{cases}.$$

Here, we have the density parameter of flat space-time is $\Omega_k = 0$. Moreover, to compute the variation between the SN Ia data and the predictions of our model, we need the luminosity distance $D_l(z)$ and the chi square function. Pantheon datasets requires the χ_{SN}^2 function in the form of,

$$\chi_{SN}^2(\alpha, \beta, \Omega_{m0}, \Omega_{\phi0}) = \sum_{i=1}^{1048} \frac{[\mu^{th}(\alpha, \beta, \Omega_{m0}, \Omega_{\phi0}) - \mu^{obs}(z_i)]^2}{\sigma_{\mu(z_i)}^2}, \quad (22)$$

where $\sigma_{\mu(z_i)}^2$ stands for the standard error of the observed value.

C. BAO datasets

The study of baryonic acoustic oscillations takes place in the early universe, when baryons and photons are inextricably linked thanks to Thomson scattering. Due to the high pressure of photons, both baryons and photons operate as a single fluid that cannot collapse under gravity but rather oscillates and gives the name to these oscillations as Baryonic acoustic oscillations (BAO). The BAO entails calculating the structural distribution of galaxies to control the rate at which cosmic structure grows throughout the universe's overall expansion. This difference, in theory, can discriminate between different forms of DE. Galaxy clustering patterns are based on statistics that describe how little discrepancies in cosmic structure are magnified. This clustering encodes a significant average parting among galaxies, which might be used to reconstruct the universe's expansion history in the same way as supernovae type Ia (standard candles) are used. The sound horizon r_s , when a photon decouples at the redshift z_* , regulates the characteristic scale of BAO, which is delivered as,

$$r_s(z_*) = \frac{c}{\sqrt{3}} \int_0^{\frac{1}{1+z_*}} \frac{da}{a^2 H(a) \sqrt{1 + (3\Omega_{0b}/4\Omega_{0\gamma})a}}.$$

Here, the terms Ω_{0b} and $\Omega_{0\gamma}$ mean the physical quantities demonstrated as baryon density and photon density at present time t .

The angular diameter distance D_A and the Hubble function $H(z)$ can also be extracted using r_s (sound horizon scale of BAO). Let $\Delta\theta$ and Δz are the observed angular separation and the measured redshift separation of the BAO feature in the 2 point correlation function of the galaxy distribution on the sky is $\Delta\theta$, and of the BAO feature in the 2 point correlation function along the line of sight is Δz , then $\Delta\theta = \frac{r_s}{d_A(z)}$ where $d_A(z) = \int_0^z \frac{dz'}{H(z')}$ and $\Delta z = H(z)r_s$.

BAO datasets of $d_A(z)/DV(z_{BAO})$ are studied in the literature [73], [74], [75], [76], [77], [78] where the photon decouples at redshift $z_* \approx 1091$, $d_A(z)$ represents the co-moving angular diameter distance, and $D_V(z) = (d_A(z)^2 z / H(z))^{1/3}$ highlights the dilation scale. Table 2 shows the data that was used in this investigation.

z_{BAO}	0.106	0.2	0.35	0.44	0.6	0.73
$\frac{d_A(z_*)}{D_V(z_{BAO})}$	30.95 ± 1.46	17.55 ± 0.60	10.11 ± 0.37	8.44 ± 0.67	6.69 ± 0.33	5.45 ± 0.31

The chi square function for BAO is given by [78]

$$\chi_{BAO}^2 = X^T C^{-1} X, \quad (23)$$

where

$$X = \begin{pmatrix} \frac{d_A(z_*)}{D_V(0.106)} - 30.95 \\ \frac{d_A(z_*)}{D_V(0.2)} - 17.55 \\ \frac{d_A(z_*)}{D_V(0.35)} - 10.11 \\ \frac{d_A(z_*)}{D_V(0.44)} - 8.44 \\ \frac{d_A(z_*)}{D_V(0.6)} - 6.69 \\ \frac{d_A(z_*)}{D_V(0.73)} - 5.45 \end{pmatrix}, \quad (24)$$

and C^{-1} is the inverse covariance matrix defined in [78].

$$C^{-1} = \begin{pmatrix} 0.48435 & -0.101383 & -0.164945 & -0.0305703 & -0.097874 & -0.106738 \\ -0.101383 & 3.2882 & -2.45497 & -0.0787898 & -0.252254 & -0.2751 \\ -0.164945 & -2.45497 & 9.55916 & -0.128187 & -0.410404 & -0.447574 \\ -0.0305703 & -0.0787898 & -0.128187 & 2.78728 & -2.75632 & 1.16437 \\ -0.097874 & -0.252254 & -0.410404 & -2.75632 & 14.9245 & -7.32441 \\ -0.106738 & -0.2751 & -0.447574 & 1.16437 & -7.32441 & 14.5022 \end{pmatrix} \quad (25)$$

By minimising the chi-square, we were able to get the best fit values of the model parameters α , β , and cosmological parameters Ω_{m0} & $\Omega_{\phi0}$ as two-dimensional contour plots with $1 - \sigma$ and $2 - \sigma$ errors using the datasets presented above. The following figures show the contour plots for α , β , Ω_{m0} , $\Omega_{\phi0}$ with respect to the Hubble datasets Fig. 1, Pantheon datasets Fig. 2 and combined Hubble+Pantheon+BAO datasets Fig. 3. The model parameter values with the best fit are determined as follows: $\alpha = 1.07_{-0.55}^{+0.63}$, $\beta = 0.56_{-0.41}^{+0.33}$, $\Omega_{m0} = 0.26713_{-0.00066}^{+0.00065}$, $\Omega_{\phi0} = 0.6989_{-0.0014}^{+0.0014}$ for Hubble datasets, $\alpha = 0.95_{-0.54}^{+0.66}$, $\beta = 0.51_{-0.42}^{+0.35}$, $\Omega_{m0} = 0.26712_{-0.00065}^{+0.00065}$, $\Omega_{\phi0} = 0.6989_{-0.0014}^{+0.0014}$ for Pantheon datasets and $\alpha = 0.998_{-0.47}^{+0.56}$, $\beta = 0.49_{-0.40}^{+0.33}$, $\Omega_{m0} = 0.26714_{-0.00066}^{+0.00064}$, $\Omega_{\phi0} = 0.6989_{-0.0014}^{+0.0014}$ for combined Hubble+Pantheon+BAO datasets. The error bar charts for the aforementioned Hubble datasets are also displayed in Fig. 4 and Pantheon datasets in the Fig. 5 and compared our obtained model (Red line) with the Λ CDM model (with $\Omega_{\Lambda0} = 0.7$ and $\Omega_{m0} = 0.3$) shown in dashed line. Our model shows nice fit to both the datasets.

We now have all of the theoretical formulae as well as numerical values for the model parameters, and we can examine the model's physical dynamics. As a result, the physical dynamics of the other essential cosmological parameters will be discussed in the next section.

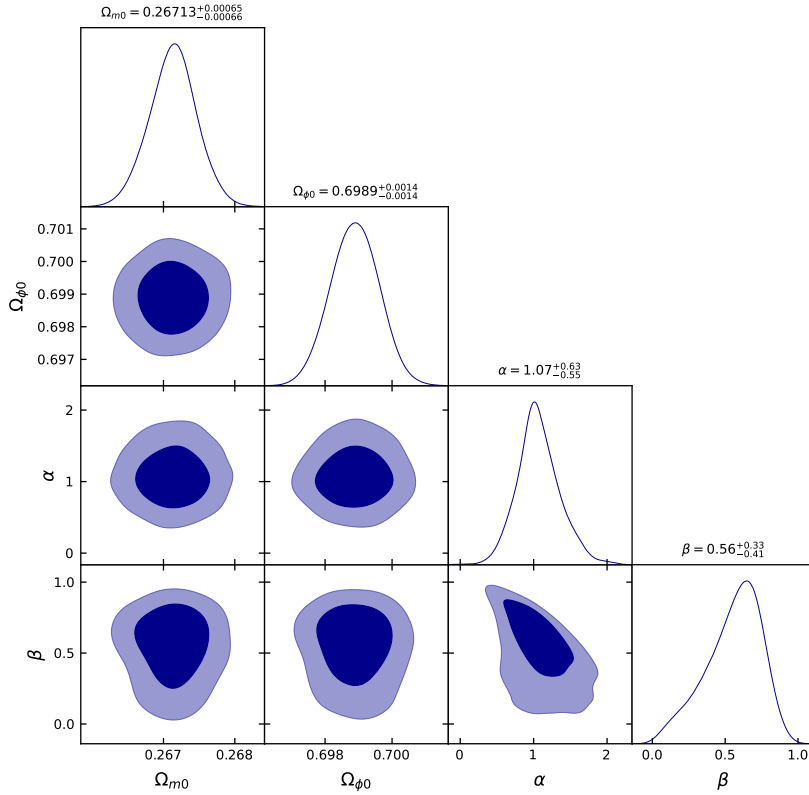


FIG. 1. The plot shows the two dimensional contour plot of the four model parameters α , β , Ω_{m0} , $\Omega_{\phi0}$ of our model with $1 - \sigma$ and $2 - \sigma$ errors and shows the best fit values of α , β , Ω_{m0} , $\Omega_{\phi0}$ with respect to the 57 points of Hubble datasets as compiled in [71].

VI. PHYSICAL DYNAMICS OF THE MODEL

The physical dynamics of the obtained model can be explained through the behavior of physical and geometrical parameters. So, in this section, we will discuss the behavior of the important cosmological parameters in the late times and future.

A. Deceleration parameter

The deceleration parameter $q < 0$ indicates that the Universe is expanding at a faster pace, whereas $q > 0$ indicates that it is slowing down. The decelerating phase is important in the cosmic evolution for the structure formation in the Universe, and the accelerating phase in the late Universe can explain the SNe Ia data. That means there must be a phase of transition ($q = 0$). In our model, the expression for the deceleration parameter $q = -\frac{\ddot{a}a}{\dot{a}^2} = -1 + \left(\frac{1+z}{H}\right) \frac{dH}{dz}$ in terms of redshift z , involving the model parameters α , β , Ω_{m0} , $\Omega_{\phi0}$ is given by,

$$q(z) = -1 +$$

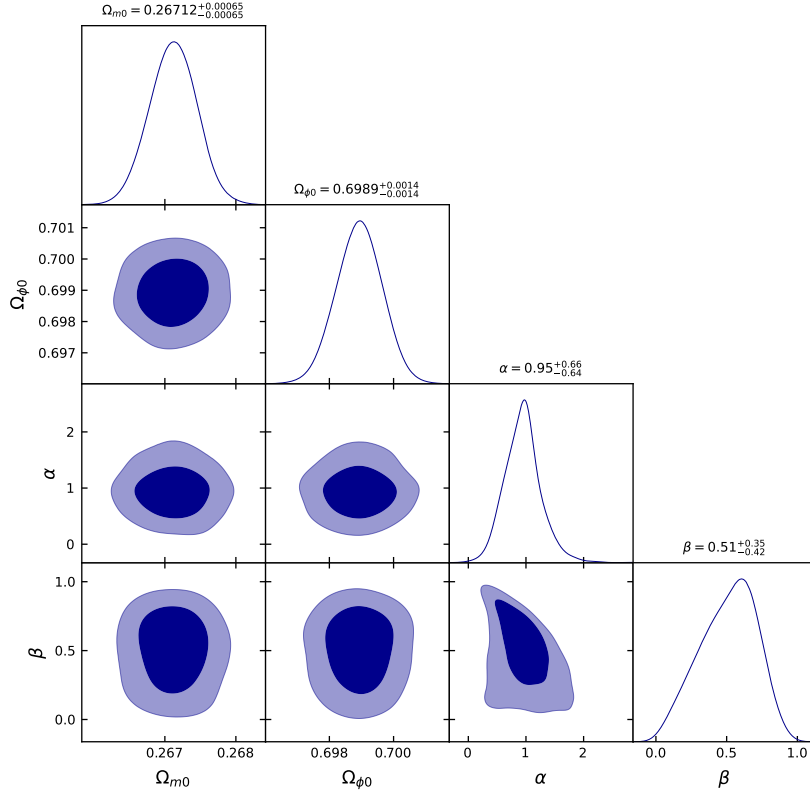


FIG. 2. The plot shows the two dimensional contour plot of the four model parameters α , β , Ω_{m0} , $\Omega_{\phi0}$ of our model with $1 - \sigma$ and $2 - \sigma$ errors and shows the best fit values of α , β , Ω_{m0} , $\Omega_{\phi0}$ with respect to the 1048 points of Pantheon datasets as compiled in [72].

$$\frac{(1+z) \left\{ 3\Omega_{m0}(1+z)^2 + \Omega_{\phi0}(1+z)^{-\beta} \text{sech}^{-1}(\beta)^{-\alpha} \cosh^{-1}\left(\frac{1+z}{\beta}\right)^\alpha \left(\frac{\alpha}{\sqrt{\frac{1+z-\beta}{1+z+\beta}} (1+z+\beta) \cosh^{-1}\left(\frac{1+z}{\beta}\right)} - \frac{\beta}{1+z} \right) \right\}}{2 \left\{ \Omega_{m0}(1+z)^3 + \Omega_{\phi0}(1+z)^{-\beta} \text{sech}^{-1}(\beta)^{-\alpha} \cosh^{-1}\left(\frac{1+z}{\beta}\right)^\alpha \right\}} \quad (26)$$

The graphic below depicts the evolution of the deceleration parameter, which describes the late evolution of a phase transition including early slowdown and late acceleration.

In the Fig. 6, the left panel (a) highlights the recent past and future evolution Hubble parameter H . The future evolution is distinct from that of standard scenario. Similarly, the right panel (b) shows the evolution of the deceleration parameter q indicating decelerating expansion in the past with a phase transitions at $z \approx 0.79$. The Universe then accelerates for an extended length of time owing to dark energy dominance. The accelerating phase of expansion in our model corresponds to the data, and this phase will continue until $z \approx -0.29$. From the plot of deceleration parameter, we can see a different behavior of the Universe from the standard lore. The deceleration parameter becomes zero at $z \approx -0.29$ and becomes positive afterwards which infers that the Universe start to contract and collapse to a *Big Crunch* singularity.

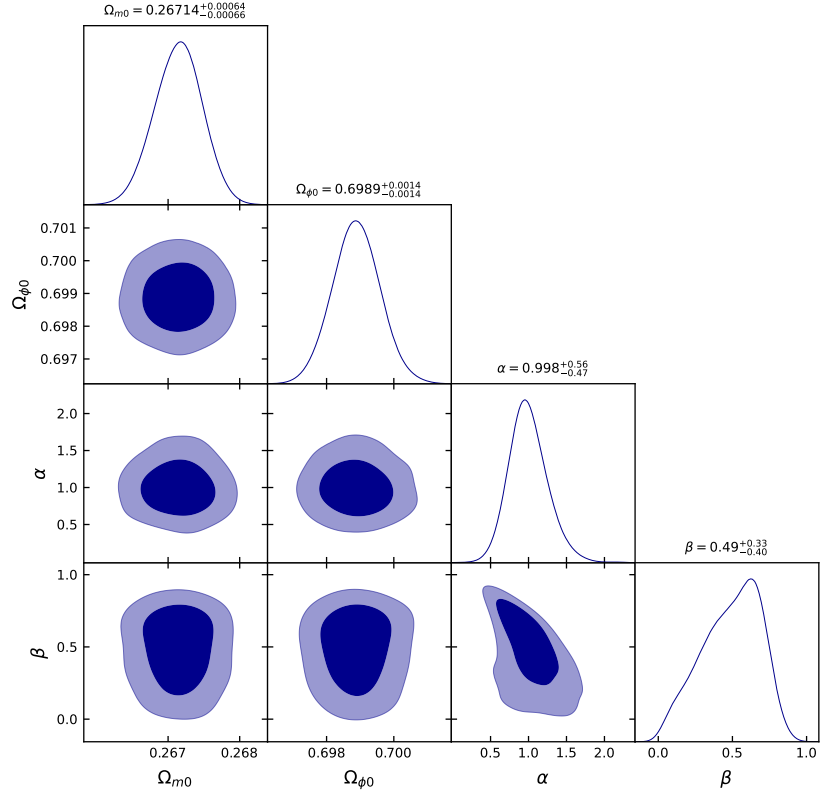


FIG. 3. This plot shows the 2 – D contour plot of the four model parameters $\alpha, \beta, \Omega_{m0}, \Omega_{\phi0}$ of our model with 1 – σ and 2 – σ errors and shows the best fit values of $\alpha, \beta, \Omega_{m0}, \Omega_{\phi0}$ with respect to the combined Hubble [71], Pantheon [72] and BAO [78] datasets.

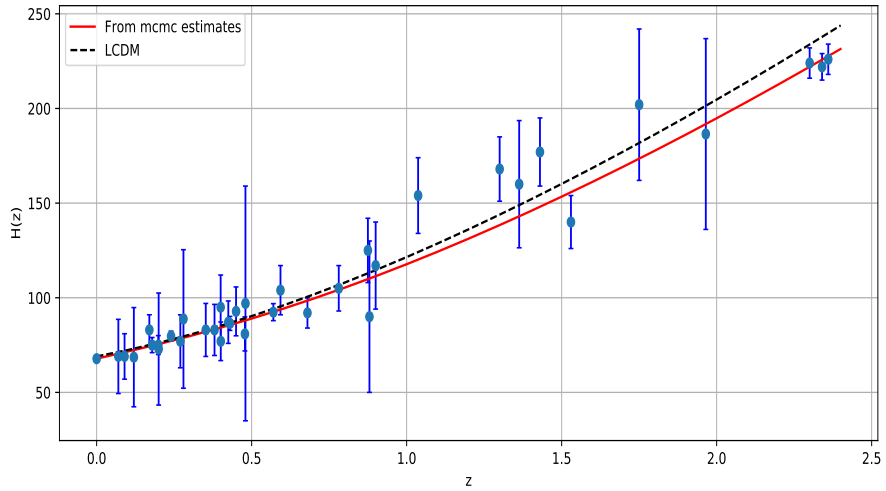


FIG. 4. The plot of Hubble function $H(z)$ vs. redshift z for our obtained model with the best fit values of the model parameters and compared with the Λ CDM model showing nice fit to the 57 points of the considered Hubble datasets with errorbars.

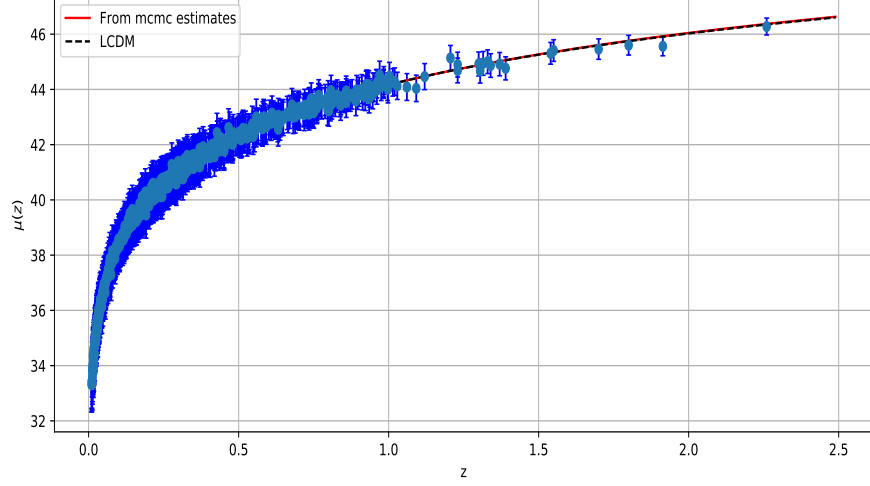


FIG. 5. The plot of $\mu(z)$ vs. z for our obtained model with the best fit values of the model parameters and compared with the Λ CDM model showing nice fit to the 1048 points of the considered Pantheon datasets with errorbars.

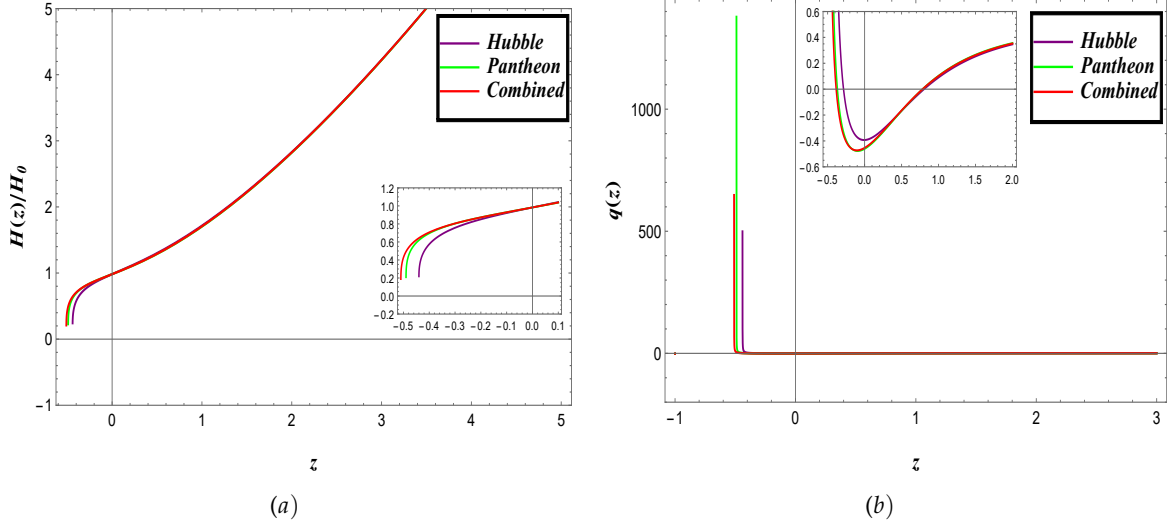


FIG. 6. In the figure the left panel (a) shows the evolution of the Hubble parameter H vs. redshift z and the right panel (b) shows the evolution of the deceleration parameter q vs. redshift z for the different sets of best fitted values of the model parameters $\alpha, \beta, \Omega_{m0}, \Omega_{\phi0}$ obtained from different observational datasets.

B. Evolution of energy densities & pressure

The evolution of matter and dark energy energy densities, as well as the pressure of dark energy, is depicted in Fig. 7 based on the values of model parameters derived from three distinct statistical studies. The first panel (a) exhibits the role of the energy density of matter which is initially very high and tends to zero in the near future. The second panel (b) shows the behavior of the dark energy density ρ_ϕ , which is high in the past, decreases in a concave downward way as time departed and finally tends to 0 as expected from the above discussions of Hubble and deceleration parameters. The third panel (c) highlights the profile of pressure of dark energy (scalar field). Initially, p_ϕ is negative, and assumes a highly positive value in the future showing a contracting phase and collapse to a big crunch.

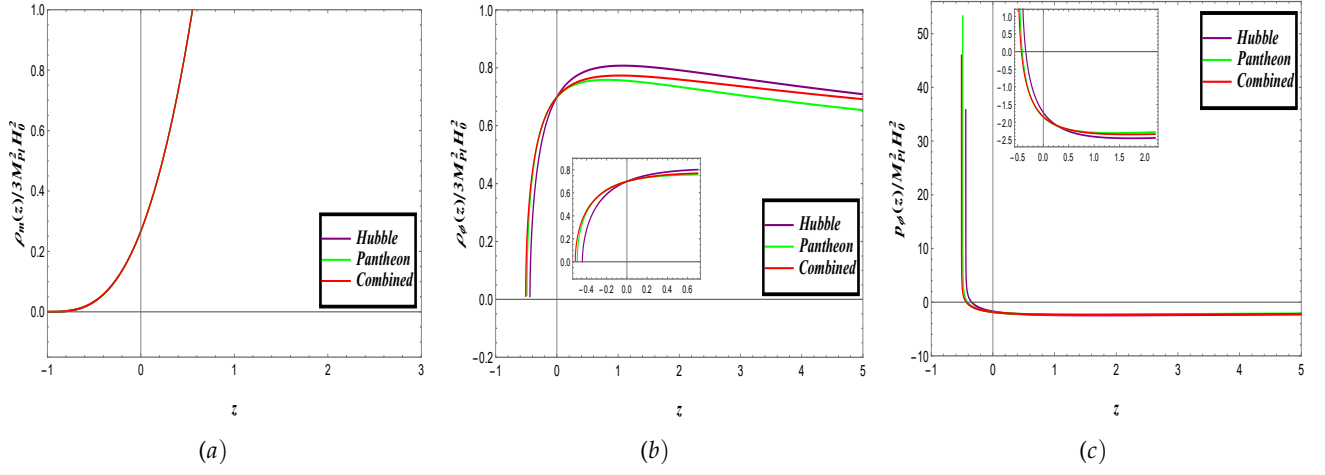


FIG. 7. The figure shows the plots of energy density of matter ρ_m , energy density of scalar field ρ_ϕ and pressure p_ϕ for our obtained model in three different panels. The three different lines shown in different colors are our models for different sets of values of model parameters.

C. EoS parameter

The expressions for the equation of state parameter $\omega_{Total} = \frac{p_{Total}}{\rho_{Total}} = \frac{2q-1}{3}$ and $\omega_\phi = \frac{p_\phi}{\rho_\phi} = \frac{M_{pl}^2 H^2 (2q-1)}{3M_{pl}^2 H^2 - \rho_m}$ are obtained in terms of redshift z , involving the model parameters α , β , Ω_{m0} and $\Omega_{\phi0}$ are given by,

$$\omega_\phi(z) = \frac{\alpha(1+z) - (3+\beta)\sqrt{\frac{1+z-\beta}{1+z+\beta}}(1+z+\beta)\cosh^{-1}\left(\frac{1+z}{\beta}\right)}{3\sqrt{\frac{1+z-\beta}{1+z+\beta}}(1+z+\beta)\cosh^{-1}\left(\frac{1+z}{\beta}\right)} \quad (27)$$

$$\omega_{Total}(z) = \frac{\Omega_{\phi0}\cosh^{-1}\left(\frac{1+z}{\beta}\right)^{\alpha-1}\left(\alpha(1+z) - (3+\beta)\sqrt{\frac{1+z-\beta}{1+z+\beta}}(1+z+\beta)\cosh^{-1}\left(\frac{1+z}{\beta}\right)\right)}{3\sqrt{\frac{1+z-\beta}{1+z+\beta}}(1+z+\beta)\left(\Omega_{m0}(1+z)^{3+\beta}\text{sech}^{-1}(\beta)^\alpha + \Omega_{\phi0}\cosh^{-1}\left(\frac{1+z}{\beta}\right)^\alpha\right)} \quad (28)$$

In the Fig. 8 the left panel (a) shows the redshift evolution of ω_ϕ , where it can be observed that the present value of ω_ϕ , $\omega_{\phi0}$ for different observational statistical datasets is ≈ -0.85 , which represents that ω_ϕ remains in quintessence region at present and is consistent with Riess [2]. Fig (b) depicts the class of ω_{total} and predicts its present evolution in the quintessence regime and becomes positive ($\omega_{total} > 0$) in the near future scenario. This observation reveals that Universe suddenly collapsed in the late times and led to Big Crunch.

D. Jerk parameter

The evidence of a rapidly expanding Universe may be interpreted in a variety of ways, including examining the behaviour of some higher derivatives of the scale factor. The geometrical behaviour of the higher-order derivatives of these cosmographic parameters (a , H , or q) allows us to investigate the performance of a variety of dark energy models. Here, we try to intend the behavior of third-order derivative of scale parameter i.e. jerk parameter j given as

$$j = \frac{\ddot{a}}{aH^3}. \quad (29)$$

In terms of redshift z , the jerk parameter j can be written as,

$$j(z) = -q + 2q(1+q) + (1+z)\frac{dq}{dz}. \quad (30)$$

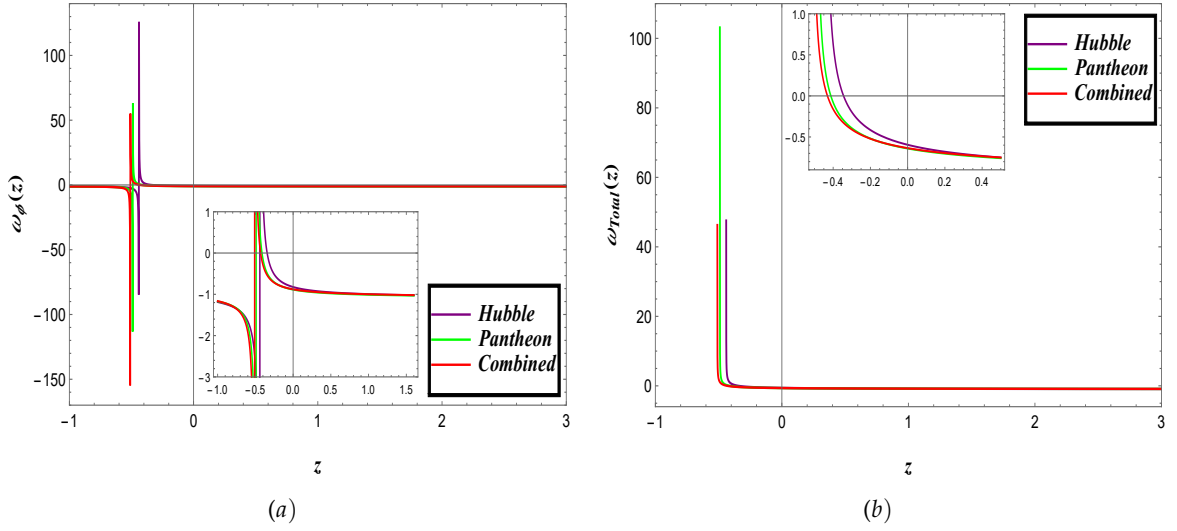


FIG. 8. The left panel (a) shows the evolution of EoS parameter of dark energy ω_ϕ vs. redshift z and the right panel (b) shows the evolution of total EoS parameter ω_{Total} vs. redshift z .

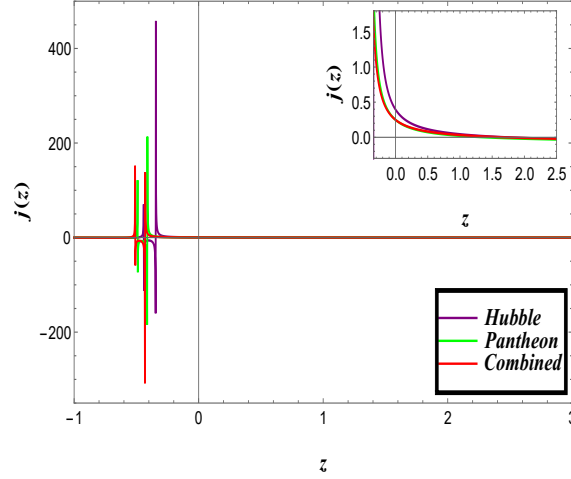


FIG. 9. The evolution of jerk Jerk parameter j vs. redshift z .

The following plot shows the evolution of the jerk parameter

From the above Fig. 9, the plot of $j(z)$, it can be noticed that initially, $j \approx 1$ and as time goes by, the value of j decreases for all three datasets. The current value of j i.e. $j_0 \approx 0$ for Hubble dataset and for pantheon it is observed to be $j_0 \approx 0.2$. The obtained value of both datasets deviates from the value of the jerk parameter, which is $j_0 = 1$ as per the standard Λ CDM model. This deviation of the observed and obtained value of j suggests that our dark energy model has contrasting aspects as to the standard Λ CDM model.

E. Statefinder diagnostic

The Hubble parameter H and the deceleration parameter q are two of the most ancient geometric parameters that describe the development of the Universe. In order to distinguish the different dark energy models and understand their behavior, few other geometric parameters are considered by the theoreticians. The pair of geometric quantities known as statefinder diagnostic parameters (s, r) and (q, r) have been proposed by V. Sahni et al. [79], which are

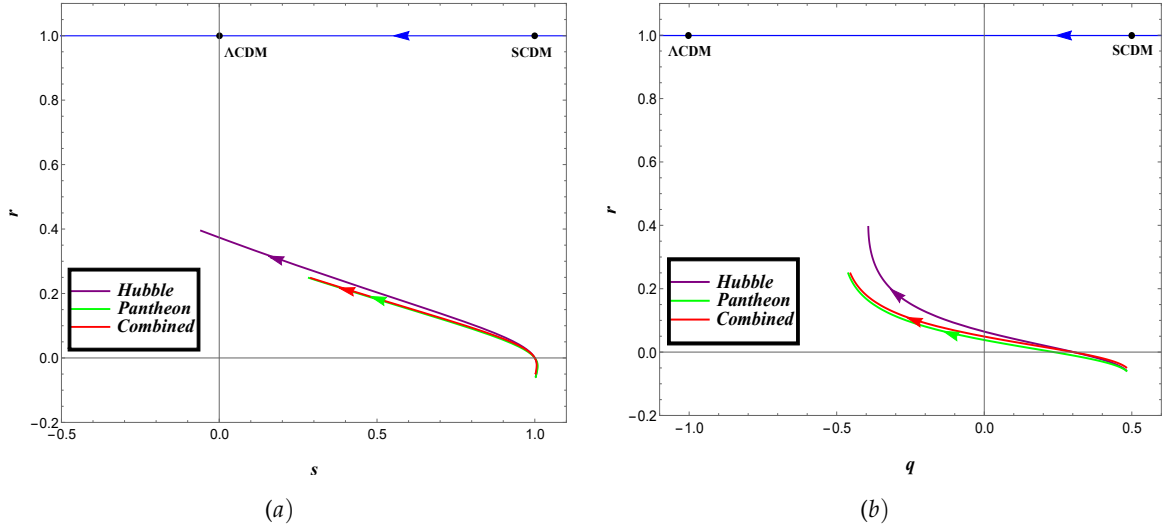


FIG. 10. In the figure the left panel (a) shows the $s-r$ plane and the right panel (b) shows the $q-r$ plane, where the dark energy model shows its evolution.

higher order derivatives of the cosmic scale factor and are similar to that of H and q . These parameters are defined as, $r = \frac{\ddot{a}}{aH^3}$, $s = \frac{r-1}{3(q-\frac{1}{2})}$ which can also be represented in terms of redshift z as,

$$r = 1 - 2\frac{1+z}{H} \frac{dH}{dz} + \frac{(1+z)^2}{H^2} \left(\frac{dH}{dz}\right)^2 + \frac{(1+z)^2}{H} \frac{d^2H}{dz^2}$$

$$s = \frac{-2\frac{1+z}{H} \frac{dH}{dz} + \frac{(1+z)^2}{H^2} \left(\frac{dH}{dz}\right)^2 + \frac{(1+z)^2}{H} \frac{d^2H}{dz^2}}{3\left(\frac{1+z}{H} \frac{dH}{dz} - \frac{3}{2}\right)}$$

The numerous trajectories in the $s-r$ and $q-r$ planes show the chronological evolution of several dark energy concepts. Few fixed points in these planes are $(s, r) = (0, 1)$, $(q, r) = (-1, 1)$ for Λ CDM model and $(s, r) = (1, 1)$, $(q, r) = (0.5, 1)$ for SCDM (standard cold dark matter) model. The deviations of any dark energy model are then evaluated from these fixed locations. For our obtained model, we have shown the (s, r) and (q, r) diagrams in the following plots.

The above (s, r) and (q, r) diagrams shown in Fig. 10 describe the nature of the dark energy. As expected, the model has large deviation from the Λ CDM model in the future.

F. Om diagnostic

A diagnostic tool known as Om diagnostic [80] has been utilized in addition to several ways to quantify the contrast of the Λ CDM model among various DE models. This method discriminates between different DE models without taking into account the EoS parameter ω . It looks at how different trajectories of $Om(z)$ behave with regard to redshift z and it can be assessed by considering H w.r.t. z . The form of $Om(z)$ is

$$Om(z) = \frac{\left\{\frac{H(z)}{H_0}\right\}^2 - 1}{(1+z)^3 - 1}. \quad (31)$$

For our model, the Om diagnostic analysis is shown in the following Fig. ??.

The action of the DE model is decided by the slope of the function $Om(z)$. The positive and negative curvature of $Om(z)$ w.r.t. z represent phantom and quintessence DE model. The zero curvature of $Om(z)$ represents the

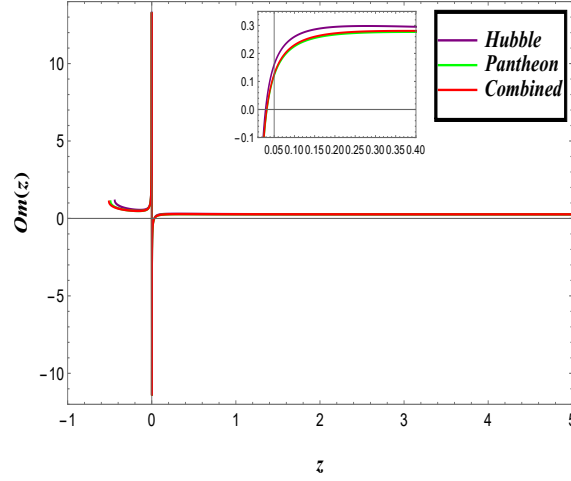


FIG. 11. The plot of Om diagnostic $Om(z)$ vs. redshift z .

standard Λ CDM model. In the plot of Om diagnostic, the trajectories are initially increasing as redshift z decreases, which means that Om has negative curvature, which corresponds to the quintessence dark energy model. Once the trajectories attained the highest value, near to $z \approx 0$, the pattern of the trajectories suddenly falls to a negative amount.

G. Energy Conditions

In GR, several conditions inhibit some regions where energy density becomes negative to acquire the realistic model of the Universe. These conditions are noticed as energy conditions. Many extensive applications of energy conditions also serve to examine the viability of some crucial singularity issues associated with the area of GR, worm holes, and black holes etc. The standard energy conditions in GR in terms of energy density ρ and pressure p are specified as:

- Weak energy condition (WEC) *i.e.*, $\rho \geq 0, \rho + p_i \geq 0$, where $i = 1, 2, 3$,
- Null energy condition (NEC) *i.e.*, $\rho + p_i \geq 0$, where $i = 1, 2, 3$,
- Strong energy condition (SEC) *i.e.*, $\rho + \sum_{i=1}^3 p_i \geq 0, \rho + p_i \geq 0$, where $i = 1, 2, 3$,
- Dominant energy condition (DEC) *i.e.*, $\rho \geq 0, \rho \geq |p_i|, \forall i$, where $i = 1, 2, 3$.

From the plots of energy conditions shown in Fig. ??, one can notice that null and dominant energy conditions are fascinated. Still, the strong energy condition is turned off, corresponding to the Universe's accelerating expansion. The achievement of null and dominant energy conditions on this version is fairly the requisite requirement to impose conditions that make the positive energy density in the Universe. However, the infraction of $\rho + 3p > 0$ suggests the presence of exotic matter in the Universe.

VII. CONCLUSION

We examined a dark energy cosmological model in the general theory of relativity in depth in this essay. As a generic scalar field, dark energy is considered as a contender. To find a consistent solution, we have taken an appropriate parametrization of density parameter of dark energy ρ_ϕ . The obtained results are considered interesting in many respects and represent two smooth transitions from decelerating phase to an accelerating one at redshift

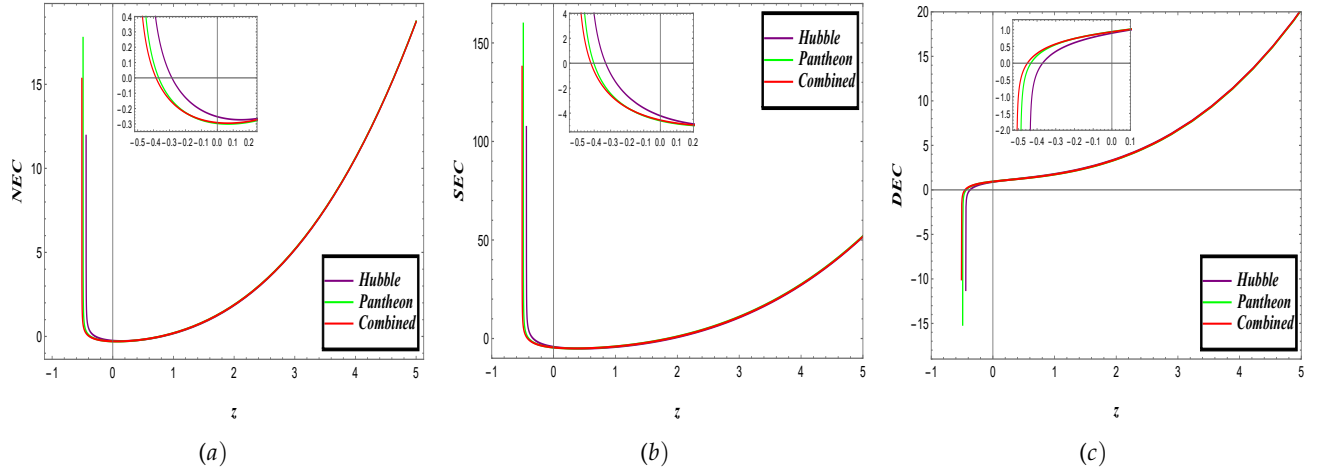


FIG. 12. The plots of energy conditions NEC, SEC and DEC for the model.

$z \approx 0.79$ in the recent past and then again from acceleration to deceleration in the future at redshift $z \approx -0.29$. The Universe's second phase transition causes the Universe to constrict and collapse into a *Big Crunch* singularity (see Fig. 6). To examine the evolution in the early phase of the Universe and to study the different stages in the cosmic evolution of the Universe, we have remolded a vital cosmic parameter (EoS parameter) in terms of deceleration parameter in FLRW background. External datasets with updated lists, such as *Hubble*, *Pantheon*, and *BAO*, were utilised to constrain the model parameters and achieve the best fit values of model parameters in the functional form of the parametrization approach employed here. The major goal of this work is to investigate the dynamics of the current speeding cosmos using a scalar field as a candidate of dark energy in the context of the FLRW metric. As a result, the major findings of our model have been recorded as follows.

- To understand the cosmic evolution, the expressions of some important cosmological parameters have been drafted as a function of redshift ' z ' and shown them graphically. The obtained model is also compared with the Λ CDM model.
- The plots in Fig. 1, Fig. 2 and Fig. 3 shown are the $2 - d$ contour plots showing best fit values of $\alpha, \beta, \Omega_{m0}, \Omega_{\phi0}$ obtained from emcee codes for the observational *Hubble*, *Pantheon* and combined *Hubble + Pantheon + BAO* datasets with $1 - \sigma$ and $2 - \sigma$ errors.
- The plots in Fig. 4 and Fig. 5 ($H(z) \sim z$ and $\mu(z) \sim z$) show the fitting of our model and compared with the Λ CDM model together with the error bars for the 57 points and 1048 of the considered Hubble datasets and Pantheon datasets.
- In the Fig. 7, the evolution of energy densities of matter, dark energy, and the pressure of dark energy are shown according to the values of the model parameters obtained. We can see the distinct behavior of the dark energy density and pressure from the standard lore. The density vanishes in the future with the increase in pressure positively showing the slowing down of expansion of the Universe and finally collapse to a Big Crunch.
- The plots in the Fig. 8(a) indicates the redshift evolution of ω_{ϕ} and ω_{total} . It has been observed that the present value of ω_{ϕ} for considered statistical datasets in the range of -0.85 approximately, which enact that ω_{ϕ} is in the quintessence region at present and is consistent with Riess [2]. The Fig. 8(b), which predicts the evolution of ω_{total} is negative at present and becomes positive in the future. This observation reveals that Universe collapses in the future and led to Big Crunch.
- Fig. 9 depict that, the deviation of the observed and obtained value of jerk parameter $j(z)$ suggests that our dark energy model has contrasting aspects as to the standard Λ CDM model.

- Fig. 10 depict the nature of the dark energy model. The obtained model is in the quintessence region at present and show a large deviation from the standard Λ CDM model in the future as the model is a collapsing one.
- From the plot shown in Fig. ?? of Om diagnostic, it can be noticed that the trajectories are initially increasing as redshift z decreases, which means that Om diagnostic has negative curvature, and corresponds to the quintessence model of DE. Once the trajectories attained the highest value, near to present time, the pattern of the trajectories suddenly falls and approaches a negative value.
- From the plots of energy conditions in Fig. ??, one can notice that NEC and DEC are fulfilled but SEC is not. The disagreement of SEC corresponds to the accelerating cosmic expansion due to the presence of exotic matter in the Universe.

After considering the aforementioned points, we can conclude that our research reveals a cosmological model that is very impressed with the approach of parametrization reconstruction of some physical parameters and saves a reasonable domain of knowledge for understanding various cosmological scenarios directly from the beginning of the Universe's evolution. Without a doubt, using some observational datasets in this work offers model parameters a more precise range, allowing for a more thorough investigation of geometrical and physical aspects. However, the current essay is merely a first step in apprehending the nature of dark energy.

ACKNOWLEDGMENTS

- [1] Ivan Debono, George F. Smoot, *Universe* **2** 23 (2016)
- [2] A. G. Riess, et al., *Astron. J.* **116** 1009 (1998)
- [3] S. Perlmutter et al., *Astrophys. J.* **517** 565 (1999)
- [4] M. Tegmark et al., *Phys. Rev. D* **69** 103501 (2004)
- [5] G. Hinshaw et al., *Astrophys. J. Suppl.* **208** 19 (2013)
- [6] B. M. Rose et al., *Astrophys. J. Lett.*, **896(1)** L4 (2020); and the references therein.
- [7] A. H. Jaffe et al., *Phys. Rev. Lett.* **86**, 3475 (2001)
- [8] D. N. Spergel et al., *Astrophys. J. Suppl.* **170**, 377 (2007)
- [9] Y. Wang and P. Mukherjee, *Astrophys. J.* **650**, 1 (2006)
- [10] U. Seljak et al., *Phys. Rev. D* **71**, 103515 (2005)
- [11] J. K. Adelman-McCarthy et al., *Astrophys. J. Suppl.* **162**, 38 (2006)
- [12] S. Weinberg, *Rev. Mod. Phys.* **61** 1 (1989)
- [13] P. J. Steinhardt, L. M. Wang and I. Zlatev, *Phys. Rev. D* **59** 123504 (1999)
- [14] C. Wetterich, *Astron. and Astrophys.* **301** 321-328 (1995)
- [15] P. J. Peebles and R. Ratra, *Astrophys J.* **325** L17 (1988)
- [16] E. J. Copeland, M. Sami and S. Tsujikawa, *Int. J. Mod. Phys. D* **15** 1753-1936 (2006); and the references therein.
- [17] I. Zlatev, L.M. Wang and P. J. Steinhardt, *Phys. Rev. Lett.* **82** (1999) 896
- [18] P. Brax and J. Martin, *Phys. Rev. D* **61** (2000) 103502
- [19] T. Barreiro, E.J. Copeland and N.J. Nunes, *Phys. Rev. D* **61** 127301 (2000)
- [20] R. R. Caldwell, *Phys. Lett. B* **545**, 23 (2003)
- [21] S. Nojiri and S. D. Odintsov, *Phys. Lett. B* **562** 147 (2003)
- [22] Parampreet Singh, M. Sami and Naresh Dadhich, *Phys. Rev. D* **68** 023522 (2003)
- [23] M. Sami and A. Toporensky, *Mod. Phys. Lett. A* **19** 1509 (2004)
- [24] C. Armendariz-Picon, T. Damour, and V. Mukhanov, *Phys. Lett. B* **458** 219 (1999)
- [25] T. Chiba, T. Okabe and M. Yamaguchi, *Phys. Rev. D* **62** 023511 (2000)
- [26] T. Chiba, T. Okabe and M. Yamaguchi, *Phys. Rev. D* **62** 023511 (2000)
- [27] C. Armendariz-Picon, V. Mukhanov and P.J. Steinhardt, *Phys. Rev. Lett.* **85** 4438 (2000)
- [28] B. Feng, X. L. Wang and X. M. Zhang, *Phys. Lett. B* **607** 35 (2005)
- [29] Z. K. Guo, Y. S. Piao, Y. Z. Zhang and X. M. Zhang, *Phys. Lett. B* **608** 177 (2005)
- [30] M. R. Setare, J. Sadeghi and A. R. Amani, *Phys. Lett. B* **660** 299 (2008)
- [31] A. Sen, *J. High Energy Phys.*, **0204** 048 (2002)

- [32] M. R. Garousi, Nucl. Phys. B **584** 284 (2000)
- [33] E. A. Bergshoeff et al., J. High Energy Phys. **5** 009 (2000)
- [34] J. Khoury, and A. Weltman, Phys. Rev. Lett. **93** 171104 (2004)
- [35] P. Brax, et al., Phys. Rev. D **70** 123518 (2004)
- [36] Abdussattar and S. R. Prajapati, Int. J. Theor. Phys. **50** 2355 (2011)
- [37] A. De Felice and S. Tsujikawa, J. Cosmol. Astropart. Phys. **03** 025 (2012)
- [38] A. Ali, R. Gannouji and M. Sami, Phys. Rev. D **82** 103015 (2010)
- [39] M. Shahalam, S. K. J. Pacif and R. Myrzakulov, Eur. Phys. J. C **76** 410 (2016)
- [40] V. Gorini et al., Phys. Rev. D **67**, 063509 (2003)
- [41] P. H. Chavanis, Eur. Phys. J. Plus **129** 38 (2012)
- [42] A. A. Starobinsky, J. Exp. Theor. Phys. Lett. **68** 757 (1998)
- [43] S. K. J. Pacif, Eur. Phys. J. Plus. **135** 792 (2020)
- [44] S. K. J. Pacif, Simran Arora, P. K. Sahoo, Phys. Dark Univ. **32** 100804 (2021)
- [45] Sanjay Mandal, Snehasish Bhattacharjee, S. K. J. Pacif, P.K. Sahoo, Phys. Dark Univ. **28** 100551 (2020)
- [46] Sanjay Mandal, P.K. Sahoo, Phys. Lett. B **823** 136786 (2021)
- [47] Raja Solanki, S. K. J. Pacif, Abhishek Parida, P. K. Sahoo, Phys. Dark Univ. **32** 100820 (2021)
- [48] J. K. Singh, Ritika Nagpal, Eur. Phys. J. C **80** (4) 295 (2020)
- [49] Ritika Nagpal et al., Eur. Phys. J. C **78** (11) 946 (2018)
- [50] R. von Marttens et al., Phys. Dark Univ. **23** 100248 (2019)
- [51] Ankan Mukherjee, Narayan Banerjee, Phys. Rev. D **93** 043002 (2016)
- [52] D. Stern et al., J. Cosmol. Astropart. Phys. **02** 008 (2010)
- [53] J. Simon, L. Verde, R. Jimenez, Phys. Rev. D **71** 123001 (2005)
- [54] M. Moresco et al., J. Cosmol. Astropart. Phys. **08**, 006 (2012)
- [55] C. Zhang et al., Research in Astron. and Astrop. **14** 1221 (2014)
- [56] M. Moresco et al., J. Cosmol. Astropart. Phys. **05** 014 (2016)
- [57] A. L. Ratsimbazafy et al., Mon. Not. Roy. Astron. Soc. **467** 3239 (2017)
- [58] M. Moresco, Mon. Not. Roy. Astron. Soc.: Letters. **450** L16 (2015)
- [59] E. Gaztañaga, A. Cabre, L. Hui, Mon. Not. Roy. Astron. Soc. **399** 1663 (2009)
- [60] A. Oka et al., Mon. Not. Roy. Astron. Soc. **439** 2515 (2014)
- [61] Y. Wang et al., Mon. Not. Roy. Astron. Soc. **469** 3762 (2017)
- [62] C. H. Chuang, Y. Wang, Mon. Not. Roy. Astron. Soc. **435** 255 (2013)
- [63] S. Alam et al., Mon. Not. Roy. Astron. Soc. **470** 2617 (2017)
- [64] C. Blake et al., Mon. Not. Roy. Astron. Soc. **425** 405 (2012)
- [65] C. H. Chuang et al., Mon. Not. Roy. Astron. Soc. **433** 3559 (2013)
- [66] L. Anderson et al., Mon. Not. Roy. Astron. Soc. **441** 24 (2014)
- [67] N. G. Busca et al., Astron. Astrop. **552** A96 (2013)
- [68] J. E. Bautista et al. Astron. Astrophys. **603** A12 (2017)
- [69] T. Delubac et al., Astron. Astrophys. **574** A59 (2015)
- [70] A. Font-Ribera et al., J. Cosmol. Astropart. Phys. **05** 027 (2014)
- [71] G. S. Sharov, V.O. Vasiliev, Mathematical Modelling and Geometry **6** 1 (2018)
- [72] D. M. Scolnic et al., Astrophys. J. **859** 101 (2018)
- [73] C. Blake et al., Mon. Not. Roy. Astron. Soc. **418** 1707 (2011)
- [74] W. J. Percival et al., Mon. Not. Roy. Astron. Soc. **401** 2148 (2010)
- [75] F. Beutler et al., Mon. Not. Roy. Astron. Soc. **416** 3017 (2011)
- [76] N. Jarosik et al., Astrophys. J. Suppl. **192** 14 (2011)
- [77] D. J. Eisenstein et al., Astrophys. J. **633** 560 (2005)
- [78] R. Giotri et al., J. Cosm. Astropart. Phys. **1203** 027 (2012)
- [79] V. Sahni et al., JETP Lett. **77** 201 (2003)
- [80] V. Sahni, A. Shaifeloo, A.A. Starobinsky, Phys. Rev. D **78** 103502 (2008)